Optimal switching of a nanomagnet assisted by microwaves

N. Barros,[1] M. Rassam,[1] H. Jirari,[2] and H. Kachkachi[1]

[1]*LAMPS, Universit de Perpignan Via Domitia, 52 Avenue Paul Alduy, F-66860 Perpignan Cedex, France*

[2]*LPMMC, C.N.R.S-UMR 5493, Université Joseph Fourier, BP 166, F-38042 Grenoble-Cedex 9, France*

(Received 17 December 2010; revised manuscript received 17 February 2011; published 22 April 2011)

We develop an efficient and general method for optimizing the microwave field that achieves magnetization switching with a smaller static field. This method is based on optimal control and renders an exact solution for the 3D microwave field that triggers the switching of a nanomagnet with a given anisotropy and in an oblique static field. Applying this technique to the particular case of uniaxial anisotropy, we show that the optimal microwave field that achieves switching with minimal absorbed energy is modulated both in frequency and magnitude. Its role is to drive the magnetization from the metastable equilibrium position toward the saddle point and then the damping induces the relaxation to the stable equilibrium position. For the pumping to be efficient, the microwave field frequency must match at the early stage of the switching process the proper precession frequency of the magnetization, which depends on the magnitude and direction of the static field. We investigate the effect of the static field (in amplitude and direction) and of damping on the characteristics of the microwave field. We have computed the switching curves in the presence of the optimal microwave field. The results are in qualitative agreement with micro-SQUID experiments on isolated nanoclusters. The strong dependence of the microwave field and that of the switching curve on the damping parameter may be useful in probing damping in various nanoclusters.

DOI: 10.1103/PhysRevB.83.144418 PACS number(s): 75.50.Tt, 75.78.−n, 75.10.Hk

I. INTRODUCTION

Fine magnetic clusters offer tremendous challenges both in the area of fundamental science and practical applications. The main reasons for this impetus are the novel features related to their small size, such as high density storage, short-time switching,[1] and fast read-write processes. However, the small size is a drawback in many regards. The energy barrier in these systems is too small to ensure a reasonable stability, in a given energy minimum, that is necessary for practical applications at room temperature, for example, magnetic recording. This is the problem of superparamagnetism. A possible way out would be to use materials with high anisotropy and thus ensuring a high-energy barrier with the consequence that high values of the writing (or switching) fields are required. But it is still unclear how to devise such high fields operating on the scale of nanoclusters while avoiding the ensuing noise. In order to keep the size small, the energy barrier high, and the switching field small, other routes are explored and a promising one among them is provided by microwaves. Microwave-assisted magnetization switching in various magnetic systems, such as thin films, has been investigated by many groups.[2]

In fact, we have at hand a more general and fundamental issue, namely the problem of getting a system out of an energy minimum by nonlinear resonance. This has previously been addressed in many areas of physics and chemistry, especially in the context of atomic physics. For example, the dissociation of diatomic molecules by a chirped infrared laser pulse requires a much lower threshold laser intensity than with a monochromatic field.[4–6] According to the classical theory of autoresonance or the quantum theory of ladder climbing,[3,6–8] exciting an oscillatory nonlinear system to high energies is possible by a weak *chirped frequency* excitation. Moreover, trapping into resonance followed by a (continuing and stable) *phase locking* with the drive is possible if the driving frequency chirp rate is small enough. It has also been shown that a slow passage through and capture into resonance yields efficient control of the energy of the driven system.

For nanoclusters it has been shown in previous works how a monochromatic microwave (MW) pulse can, by means of a nonlinear resonance, substantially reduce the static field needed to reverse the magnetization of an individual nanoparticle.[9] The switching curves obtained in these measurements present some irregular features that depend on the MW and dc field characteristics, the potential energy of the nanomagnet, and the damping parameter. In particular, the strong dependence of these features on the damping parameter might be used to estimate the latter in such clusters.

Several theoretical works have been devoted to the understanding of the magnetization dynamics, and in particular its reversal, under the effect of a time-dependent magnetic field. The theoretical work may be divided into two kinds. The first deals with the effect of a given MW field with a given polarization[10,11] while the second seeks optimal strategies for achieving the magnetization switching.[12] In particular, a few works[13] assume a given dynamics for the magnetization and attempt to determine the MW field that realizes it.

In the present work we use a general method borrowed from the optimal control theory[14–16] and apply it to the switching of a nanocluster. This method renders an exact solution for the MW field vector necessary for the switching of a nanomagnet with a given potential energy (comprising anisotropy and an oblique static field). The standard formulation of this method consists of minimizing a cost functional using the conjugate gradient technique. The latter is known to be a local-convergence method and thus renders a solution that is rather sensitive to the initial guess. In order to acquire global convergence, we have supplemented the conjugate gradient routine by a global search using the Metropolis algorithm and simulated annealing. We have applied our algorithm to a nanomagnet in the macrospin approximation with uniaxial anisotropy and

oblique dc magnetic field. We have investigated the effect of the latter (both in direction and magnitude) and of damping on the characteristics of the MW field. Then we computed the limit-of-metastability (or switching) curves for different (small) values of damping.

II. METHOD OF OPTIMAL CONTROL APPLIED TO NANOMAGNETS

One of our objectives here is to develop a general method that allows us to solve the following inverse problem. What is the optimal time-dependent magnetic field under which the magnetization of a nanoparticle, with given potential energy, switches from a given initial state to a given final prescribed target state? After formulating this method we apply it to the case of a macrospin or a nanoparticle in the SW approximation in an energy potential composed of uniaxial anisotropy and a Zeeman contribution from an oblique dc field.

The method we propose is borrowed from the optimal control theory. The main idea is to start with an arbitrary MW magnetic field $\mathbf{h}_{\rm ac}(t)$ with its three components $h^{\alpha}_{\rm ac}$, $\alpha = x, y, z$, that we call the *control field*, in addition to the static magnetic field and anisotropy field. We then determine $\mathbf{h}_{\rm ac}(t)$ that triggers the switching of the cluster's magnetization between two given states within a prescribed interval of time.

A. Model

Consider a nanomagnet in the macrospin approximation where its magnetic state is represented by a macroscopic magnetic moment $\mathbf{m} = \mu_s \mathbf{s}$, where μ_s is its magnitude and $\mathbf{s}$ its direction with $|\mathbf{s}| = 1$. In this approximation the relevant terms entering the energy E of the nanomagnet are the magnetocrystalline anisotropy and the Zeeman energy. The applied dc (static) field $\mathbf{H}_{\rm dc}$ is assumed to point in an arbitrary direction $\mathbf{e}_h = \mathbf{H}_{\rm dc}/H_{\rm dc}$. Using the convention $\mu_0 = 1$ so that the magnetic fields are expressed in Tesla, one then defines the effective field

$$\mathbf{H}_{\rm eff} = -\frac{1}{\mu_s}\frac{\delta E}{\delta \mathbf{s}} \tag{1}$$

and writes the damped Landau-Lifshitz equation (LLE) that governs the dynamics of $\mathbf{s}$, assuming that the module μ_s remains constant,

$$\frac{1}{\gamma}\frac{d\mathbf{s}}{dt} = -\mathbf{s}\times\mathbf{H}_{\rm eff} - \alpha\,\mathbf{s}\times(\mathbf{s}\times\mathbf{H}_{\rm eff})\,, \tag{2}$$

where $\gamma \simeq 1.76\times 10^{11}$ (T s)$^{-1}$ is the gyromagnetic factor and α is the phenomenological damping parameter (taken here in the weak regime).

We measure all applied fields in terms of the anisotropy field

$$H_a = \frac{2KV}{\mu_s} \tag{3}$$

and in particular we define the reduced effective field

$$\mathbf{h}_{\rm eff} \equiv \frac{1}{H_a}\mathbf{H}_{\rm eff} = -\frac{\delta \mathcal{E}}{\delta \mathbf{s}} \tag{4}$$

with $\mathcal{E} \equiv E/(2KV)$. In terms of $\mathbf{h}_{\rm eff}$ LLE becomes

$$\frac{d\mathbf{s}}{d\tau} = -\mathbf{s}\times\mathbf{h}_{\rm eff} - \alpha\,\mathbf{s}\times(\mathbf{s}\times\mathbf{h}_{\rm eff})\,, \tag{5}$$

where $\tau \equiv t/t_s$ is the dimensionless time and $t_s = 1/(\gamma H_a)$ is the characteristic scaling time of the system. For instance, for a cobalt particle of 3-nm diameter[17] with $K \simeq 2.2\times 10^5$ J m^{-3} and $\mu_s \simeq 3.8\times 10^{-20}$ A m^2 we have $H_a \simeq 0.3$ T and $t_s \simeq 1.9\times 10^{-11}$ s.

B. Formulation of the optimal control problem

1. General procedure

The idea here is to introduce a control field $\mathbf{h}_{\rm ac}(\tau) \equiv \mathbf{H}_{\rm ac}/H_a$ and then seek its optimal form that allows for driving the magnetic moment direction $\mathbf{s}$ from the given initial state $\mathbf{s}^{(i)}$ at time $\tau_i = 0$ into the desired final state $\mathbf{s}^{(f)}$ at the given observation time τ_f. Accordingly, we replace in the LLE (5) the (deterministic) field $\mathbf{h}_{\rm eff}$ by the total (time-dependent) field

$$\boldsymbol{\zeta}(\tau) = \mathbf{h}_{\rm eff} + \mathbf{h}_{\rm ac}(\tau). \tag{6}$$

This results in the following equation of motion, which will be henceforth referred to as the driven LLE (DLLE):

$$\dot{\mathbf{s}} = -\mathbf{s}\times\boldsymbol{\zeta}(\tau) - \alpha\,\mathbf{s}\times[\mathbf{s}\times\boldsymbol{\zeta}(\tau)]\,. \tag{7}$$

The field $\mathbf{h}_{\rm ac}(\tau)$ is then determined through the minimization of a cost functional which, in the present case, may be written as

$$\mathcal{F}[\mathbf{s}(\tau),\mathbf{h}_{\rm ac}(\tau)] = \frac{1}{2}\|\mathbf{s}(\tau_f) - \mathbf{s}^{(f)}\|^2 + \frac{\eta}{2}\int_0^{\tau_f} d\tau\,\mathbf{h}^2_{\rm ac}(\tau). \tag{8}$$

The first term measures the degree at which the magnetic moment switching is achieved and vanishes in the case of full switching. The second term is quadratic in the driving field and is thus proportional to the absorbed energy. The parameter η, called the *control parameter*, allows us to balance the second condition with respect to the first.

Therefore, the problem of optimal control boils down to minimizing the cost functional (8) along the trajectory given by DLLE (7). More explicitly, this amounts to solving the following problem:

$$\begin{cases} \min\left\{\mathcal{F}[\mathbf{s},\mathbf{h}_{\rm AC}] = \frac{1}{2}\|\mathbf{s}(\tau_f) - \mathbf{s}^{(f)}\|^2 + \frac{\eta}{2}\int_0^{\tau_f} d\tau\,\mathbf{h}^2_{\rm AC}(\tau)\right\} \\ \dot{\mathbf{s}} = -\mathbf{s}\times\zeta - \alpha\,\mathbf{s}\times(\mathbf{s}\times\zeta), \quad \tau\in[0,\tau_f] \\ \mathbf{s}(0) = \mathbf{s}^{(i)}. \end{cases} \tag{9}$$

An optimal solution of this problem is characterized by the first-order optimality condition in the form of the Pontryagin minimum principle (PMP).[18] These conditions are more conveniently formulated with the help of a Hamilton function which may in the present case be written in the following form:

$$\mathcal{H}[\mathbf{s}(\tau),\boldsymbol{\lambda}(\tau),\mathbf{h}_{\rm ac}(\tau)] = \frac{\eta}{2}\mathbf{h}^2_{\rm ac}(\tau) + \boldsymbol{\lambda}(\tau)[-\mathbf{s}\times\boldsymbol{\zeta} - \alpha\mathbf{s}\times(\mathbf{s}\times\boldsymbol{\zeta})], \tag{10}$$

where $\boldsymbol{\lambda}(\tau)$, called the adjoint state variable (see below), is a Lagrange parameter introduced to implement the constraint and thereby render $\mathbf{s}(\tau)$ independent of $\mathbf{h}_{\rm ac}(\tau)$. The PMP then states that solving problem (9) is equivalent to solving the following boundary problem (i.e., the Hamilton-Jacobi

equations with boundary conditions):

$$\begin{cases} \dot{\mathbf{s}} = \frac{\delta \mathcal{H}}{\delta \lambda}, \quad \mathbf{s}(0) = \mathbf{s}^{(i)}, \quad \tau \in [0, \tau_f], \\ \dot{\lambda} = -\frac{\delta \mathcal{H}}{\delta \mathbf{s}}, \quad \lambda(\tau_f) = \mathbf{s}(\tau_f) - \mathbf{s}^{(f)}, \\ \frac{\delta \mathcal{H}}{\delta \mathbf{h}_{\rm AC}} = 0. \end{cases} \tag{11}$$

The last condition is also equivalent to the vanishing of the gradient of the cost functional $\mathcal{F}$ in Eq. (8). It yields the equation

$$\frac{\delta \mathcal{H}}{\delta \mathbf{h}_{\rm ac}} = \eta\, \mathbf{h}_{\rm ac} + \mathbf{s} \times \boldsymbol{\lambda} - \alpha\, \mathbf{s} \times (\mathbf{s} \times \boldsymbol{\lambda}), \tag{12}$$

which is used to compute the variation in the cost functional, that is,

$$\delta \mathcal{F} = \int_0^{\tau_f} d\tau\, \frac{\delta \mathcal{H}}{\delta \mathbf{h}_{\rm ac}} \delta \mathbf{h}_{\rm ac}. \tag{13}$$

In general, this problem is highly nonlinear and considering, on top of that, the nonlinearity of the Landau-Lifshitz equation, it is not possible to find analytical solutions. Consequently, we resort to numerical approaches. The advantage of this formulation is manifold. (i) The MW field $\mathbf{h}_{\rm ac}(\tau)$ is obtained in 3D, that is, one obtains the three functions of time $h^{\alpha}_{\rm ac}(\tau), \alpha = x, y, z$; and for any potential energy (anisotropy, dc field, etc.). (ii) The final time τ_f, and the absorbed power [second term in Eq. (8)] can be adjusted; the latter may be achieved by tuning the control parameter η. (iii) One can generalize this treatment to many-spin problems[19] and also include thermal effects.

One of the most efficient techniques for (numerically) solving such a minimization problem is the conjugate-gradient method. However, the drawback of this method is that it is a local-convergence method which means that the solution it renders is strongly dependent on the initial guess. We overcome this inconvenience by supplementing the method with a global search using the Metropolis algorithm with random increments and then proceed with the technique of simulated annealing.

For numerical calculations we have discretized the boundary-value problem (11) by subdividing the time interval $[\tau_i = 0, \tau_f]$ into N time slices

$$\tau_n = \tau_i + n \times \Delta\tau, \quad n = 0, \ldots, N-1, \quad \tau_f = \tau_{N-1},$$

where

$$\Delta\tau = \frac{\tau_f - \tau_0}{N-1}.$$

Then, using the notation $\mathbf{v}_n = \mathbf{v}(\tau_n)$ for a vector $\mathbf{v}$, Eqs. (7), (8), and (13) and the equation for $\boldsymbol{\lambda}$ become

$$\mathbf{s}_{n+1} = \mathbf{s}_n + \Delta\tau \times [-\mathbf{s}_n \times \boldsymbol{\zeta}_n - \alpha\, \mathbf{s}_n \times (\mathbf{s}_n \times \boldsymbol{\zeta}_n)], \quad \mathbf{s}(\tau_i) = \mathbf{s}^{(i)}, \tag{14a}$$

$$\mathcal{F} = \frac{1}{2} \|\mathbf{s}_{N-1} - \mathbf{s}^{(f)}\|^2 + \frac{\eta \Delta\tau}{2} \sum_{n=0}^{N-1} \mathbf{h}^2_{{\rm ac},n}, \tag{14b}$$

$$\boldsymbol{\lambda}_{n-1} = \boldsymbol{\lambda}_n - \Delta\tau \times \Lambda_n, \quad \boldsymbol{\lambda}_f = \mathbf{s}_{N-1} - \mathbf{s}^{(f)}, \tag{14c}$$

$$V_n = \frac{\delta \mathcal{F}}{\delta \mathbf{h}_{{\rm ac},n}} = \Delta\tau \times [\eta\, \mathbf{h}_{{\rm ac},n} + \mathbf{s}_n \times \boldsymbol{\lambda}_n - \alpha\, \mathbf{s}_n \times (\mathbf{s}_n \times \boldsymbol{\lambda}_n)]. \tag{14d}$$

The explicit expression for Λ_n in Eq. (14c) depends on the energy potential (see below for the case of uniaxial anisotropy).

We may summarize the numerical procedure as follows. (i) For a given initial guess of the control field $\mathbf{h}_{\rm ac}(t)$ we first solve the state equation (14a) forward in time using the initial condition, and then evaluate the cost functional (14b). (ii) The solution obtained for $\mathbf{s}$ is then used for the backward (since the condition now is at t_f) integration of Eq. (14c) for $\boldsymbol{\lambda}$. (iii) With the trajectories of $\mathbf{s}$ and $\boldsymbol{\lambda}$ thus obtained we compute the gradient (14d). The numerical subroutines are standard and can be found in Ref. 20. We emphasize that obtaining the control field amounts to solving for $3 \times N$ variables.

2. *Uniaxial anisotropy*

In the case of uniaxial anisotropy with oblique static field the energy of the nanomagnet reads (in units of the anisotropy energy 2 KV)

$$\mathcal{E} = -h_{\rm dc}\ (\mathbf{e}_h \cdot \mathbf{s}) - \tfrac{1}{2} (\mathbf{s} \cdot \mathbf{n})^2 \tag{15}$$

with K and $\mathbf{n}$ being the anisotropy constant and easy axis, V is the nanomagnet volume, and $h_{\rm dc} \equiv H_{\rm dc}/H_a$. The effective field explicitly reads [see Eq. (4)]

$$\mathbf{h}_{\rm eff} = h_{\rm dc}\, \mathbf{e}_h + (\mathbf{s} \cdot \mathbf{n})\, \mathbf{n}. \tag{16}$$

From the second equation in (11) we obtain the explicit equation for $\boldsymbol{\lambda}$,

$$\dot{\boldsymbol{\lambda}} = \boldsymbol{\zeta} \times \boldsymbol{\lambda} + \alpha[\boldsymbol{\zeta} \times (\boldsymbol{\lambda} \times \mathbf{s}) + \boldsymbol{\lambda} \times (\boldsymbol{\zeta} \times \mathbf{s})] + \{\boldsymbol{\lambda}[\mathbf{s} \times \mathbf{n} + \alpha\, \mathbf{s} \times (\mathbf{s} \times \mathbf{n})]\}\mathbf{n} \tag{17}$$

and in Eq. (14c) we now have

$$\Lambda_n = \boldsymbol{\zeta}_n \times \boldsymbol{\lambda}_n + \alpha[\boldsymbol{\zeta}_n \times (\boldsymbol{\lambda}_n \times \mathbf{s}_n) + \boldsymbol{\lambda}_n \times (\boldsymbol{\zeta}_n \times \mathbf{s}_n)] + [\boldsymbol{\lambda}_n + \alpha(\boldsymbol{\lambda}_n \times \mathbf{s}_n)](\mathbf{s}_n \times \mathbf{n})\mathbf{n}.$$

III. RESULTS

In the present work we have considered the case of a nanomagnet with uniaxial anisotropy and oblique static field. Unless otherwise stated, the latter is applied in the yz plane making an angle of 170° with respect to the easy axis (z axis). Its reduced magnitude is $h_{\rm dc} = 0.5$, corresponding to a field magnitude $H_{\rm dc} \simeq 150$ mT. The initial and target states $\mathbf{s}^{(i)}$ and $\mathbf{s}^{(f)}$, which correspond respectively to the metastable equilibrium state and stable equilibrium state, are computed numerically. The observation time is $\tau_f = 600$ (i.e., $t_f \simeq 11.4$ ns). The damping parameter is $\alpha = 0.05$ and the control parameter η has been set to 0.01. The static field, damping parameter, and observation time have been varied and their effects studied (see later on). For simplicity we have taken a linearly polarized MW field, that is, $\mathbf{h}_{\rm ac}(t) = h_{\rm ac}(t)\mathbf{e}_x$. This choice also suits the experimental setup.[9]

In Fig. 1 we have plotted the optimized MW field magnitude $H_{\rm ac}(t) \equiv H_a\, h_{\rm ac}(t)$ where t is the time in seconds, together with the components of the magnetic moment, that is, $s_\alpha(t), \alpha = x, y, z$. First, we note that the amplitude of the MW field is rather small as it does not exceed 15 mT, which is 10 times smaller than the static field. Moreover, the summed magnitudes of the dc and MW field are smaller than the SW switching field for the chosen dc field direction (about 200 mT). This shows that in the presence of a MW field magnetic switching is achieved at a smaller dc field. Second,

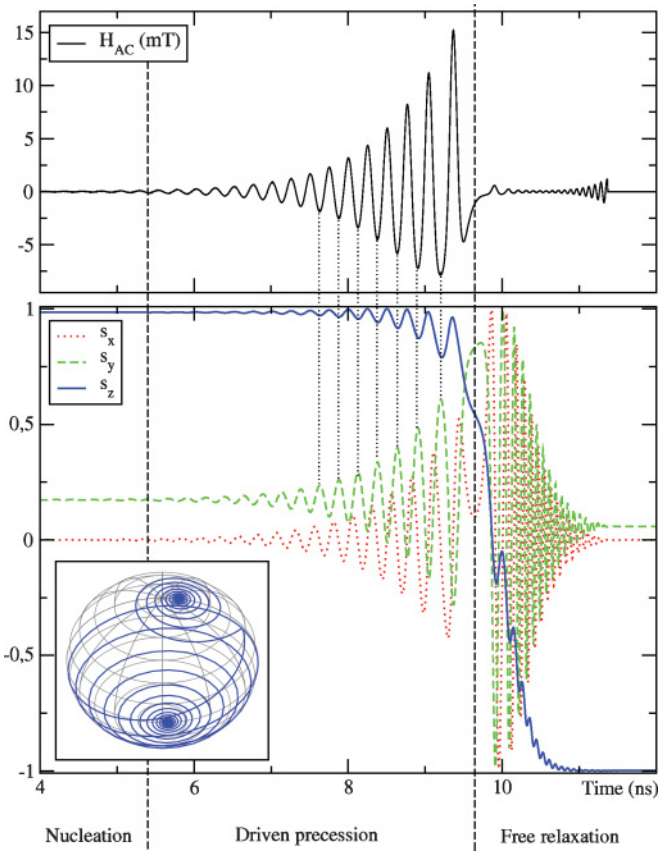

FIG. 1. (Color online) Optimized MW field (upper panel) and the corresponding spin trajectories (lower panel). The inset is a 3D plot of the spin trajectory on the unit sphere.

the striking feature is that the MW field is modulated both in amplitude and frequency. Its frequency is a slowly varying function of time in the stage that precedes switching, as can be seen in Fig. 2. Third, as is hinted to by the dashed vertical lines, the extrema in the MW field and the spin components $s_y(t)$ and $s_z(t)$ match at all times before switching. This simply implies that the magnetic moment is phase locked to the MW field. All these features agree with the predictions of the classical autoresonance or the ladder-climbing quantum theory, as summarized in the Introduction.

The instantaneous frequency has been obtained after passing the optimized MW field through the Butterworth filter and then applying the Hilbert transformation.[21,22] As can be seen for short times the instantaneous frequency oscillates around the approximate value $f_0 \approx 4.1$ GHz. This initial frequency is simply the FMR frequency given by

$$f_{\rm FMR} = \frac{\gamma H_a}{2\pi}\sqrt{h^{(i)}_{{\rm eff},\parallel}\left\{ h^{(i)}_{{\rm eff},\parallel} + k[(\mathbf{s}^{(i)}.\mathbf{n})^2 - 1]\right\}},$$

where $h^{(i)}_{{\rm eff},\parallel} \equiv \mathbf{h}_{\rm eff}{}^{(i)} \cdot \mathbf{s}^{(i)} = h_{\rm dc}(\mathbf{e}_h \cdot \mathbf{s}^{(i)}) + (\mathbf{s}^{(i)} \cdot \mathbf{n})^2$ is the effective field (16) evaluated at and then projected onto the initial position $\mathbf{s}^{(i)}$. As the magnetic moment approaches the saddle point the frequency decreases rapidly and eventually vanishes when the magnetic moment crosses the saddle point into the more stable energy minimum.

In Fig. 1 it is seen that the time span comprises three stages (for the set of physical parameters considered). (1) *Nucleation stage* (up to 5.4 ns). The MW field remains almost zero and the magnetic moment remains in the metastable state. (2) *Driven precession* (from 5.4 to 9.7 ns). Here the MW field and the magnetic moment are synchronized. At each procession cycle the MW field hooks up the magnetic moment and pushes it upward in the energy potential toward the saddle point. This is the phase-locking process mentioned in the Introduction and observed above. This is indeed possible because the frequency chirp rate is small as can be seen in Fig. 2 for $5.4 \leqslant t \leqslant 9.7$ ns. The MW field thus compensates for the effect of damping that tends to pull the magnetic moment back toward its initial position. At around 9.7 ns the magnetic moment crosses the saddle point. (3) *Free relaxation*. From 9.7 ns onward the magnitude of the MW field dwindles and the synchronization with the magnetic moment is lost. We note that at the saddle point the precession reverses from being counter-clockwise to clockwise as the magnetic moment switches to the lower half sphere.

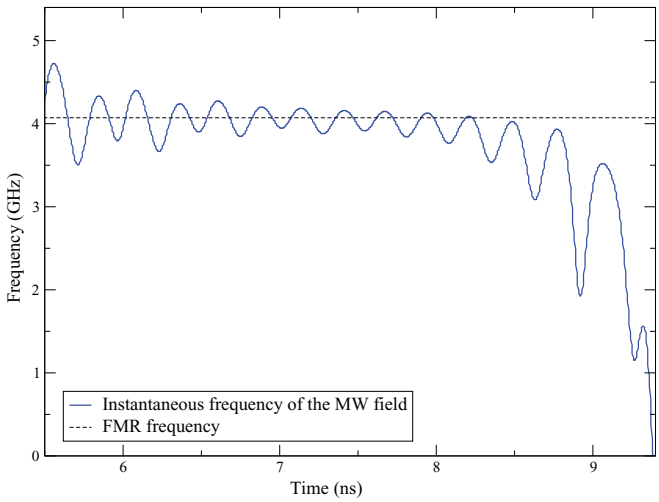

FIG. 2. (Color online) Instantaneous frequency of the optimized and filtered MW field of Fig. 1. The other parameters are the same as in Fig. 1.

Numerical tests show that the MW field can be replaced by zero during the nucleation and free relaxation stages without noticeably affecting the trajectory of the magnetic moment. This implies that the most relevant part of the signal is that during the driven precession the role of the MW field is to drive the magnetic moment toward the saddle point. Next, the damping takes up to lead it to the more stable energy minimum. During the driven precession the frequency of the MW field and the precession frequency of the magnetic moment are similar. Consequently, the magnetic moment switching can be viewed as a resonant process. The pumping by the MW field is efficient when its frequency matches the frequency of the magnetization (phase locking).

The same calculation has been carried out with the same sampling time but different values for the total observation time t_f. The results are shown in Fig. 3. If the total time is larger than an effective time of 6 ns, similar values are obtained for the cost functional and the curves $h_{\rm ac}(t)$ can be matched after a time shift. As was discussed earlier, this effective time corresponds to the sum of the time of driven precession and that of free relaxation. This result implies that the nucleation

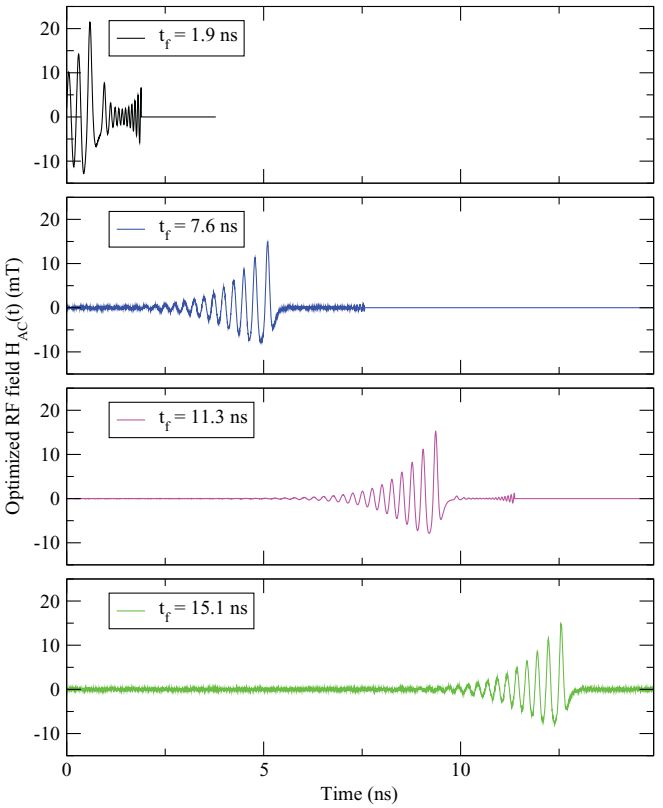

FIG. 3. (Color online) Optimized MW field obtained with four different total times t_f.

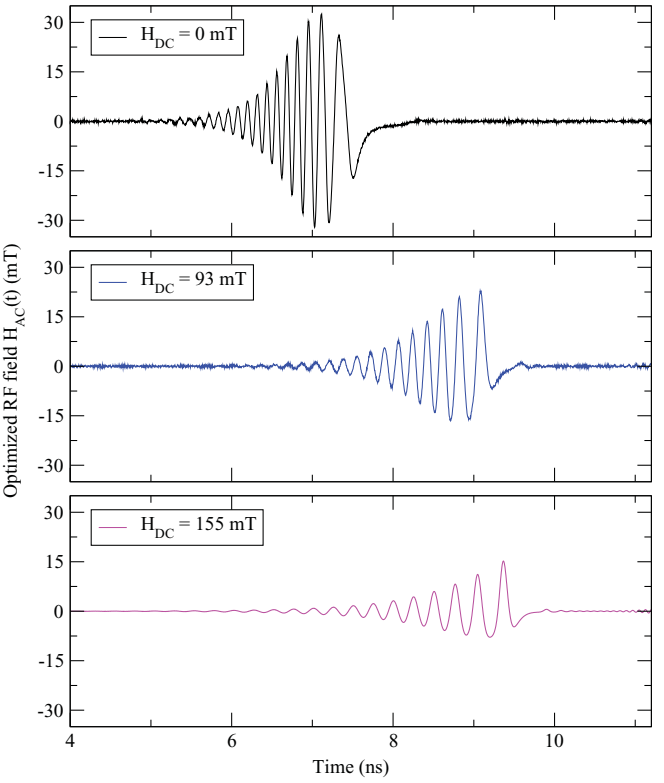

FIG. 4. (Color online) Optimized MW field obtained for different magnitudes of the static field $\mathbf{h}_{\rm dc}$ in the same direction making an angle $\theta = 170^\circ$ with respect to the anisotropy easy axis.

stage can be suppressed without affecting the final optimized MW field. However, if the total time is too short, the final value found for the cost functional is higher (i.e., not fully minimized). Indeed, we see in Fig. 3 (uppermost panel) that the stage of driven precession is shortened and the shape of the control field changes so as to achieve a faster switching and thus comply with the switching-time constraint [first term in Eq. (8)].

For comparison, we have also computed the spin trajectory with a monochromatic field instead of our optimized chirped MW field. This monochromatic field was polarized along the x axis with a constant intensity and a frequency equal to the FMR frequency in the initial energy well. We find that to achieve switching a minimal intensity of 19 mT is required, which is 4 mT higher than the maximal intensity of the optimized field. On the other hand, the monochromatic field induces a faster switching (in about 1.5 ns) but for an injected energy that is about 5 times larger than with the optimized field.

The effect of varying the amplitude of the static field on the MW field is shown in Fig. 4. We see that the shape of the MW field envelope remains the same, apart from the fact that the smaller the static field the more symmetrical is the MW field. This shows that for a higher field $h_{\rm dc}$ the energy potential is less symmetrical. Moreover, as $h_{\rm dc}$ is increased the energy barrier is lowered and the MW field required to achieve switching is smaller. Again the initial frequency of the oscillations matches the FMR frequency of the system; when $h_{\rm dc}$ increases the latter decreases. The cost functional was found to be proportional to the energy barrier between the saddle point and the metastable minimum. Hence when the energy barrier is higher more energy has to be injected in order to overcome it. The same study has been carried out upon varying the direction of the static field.

We have also investigated the effect of varying the damping parameter α on the MW field. The results are summarized in Fig. 5. We see that the intensity of the field increases with α, which is compatible with what was suggested earlier, namely that the role of the MW field is to compensate for the damping effect. This effect is similar to what happens with a rubber band. The more you stretch it the harder it becomes to do so. Moreover, the effective duration of the MW field, which mainly corresponds to the driven precession period, decreases when α increases. We note that, on the contrary, the initial frequency of the oscillations is independent of α (see Fig. 6). This result can be understood qualitatively if we suppose that, at any time, the MW field exactly compensates for the effect of damping. The spin dynamics is then governed by the undamped LLE and the magnetic moment precesses with its proper frequency, which is independent of the damping parameter. At short times, since the precession angle is small, this precession frequency is equal to the FMR frequency.

As discussed in the Introduction, one of the objectives of investigating the magnetization switching assisted by MWs is to achieve an optimal switching with smaller dc magnetic fields than it would be necessary without MWs. This means that applying the dc field in a given direction and varying its magnitude one determines the switching field (or the field at the limit of metastability) at which the magnetization is reversed.

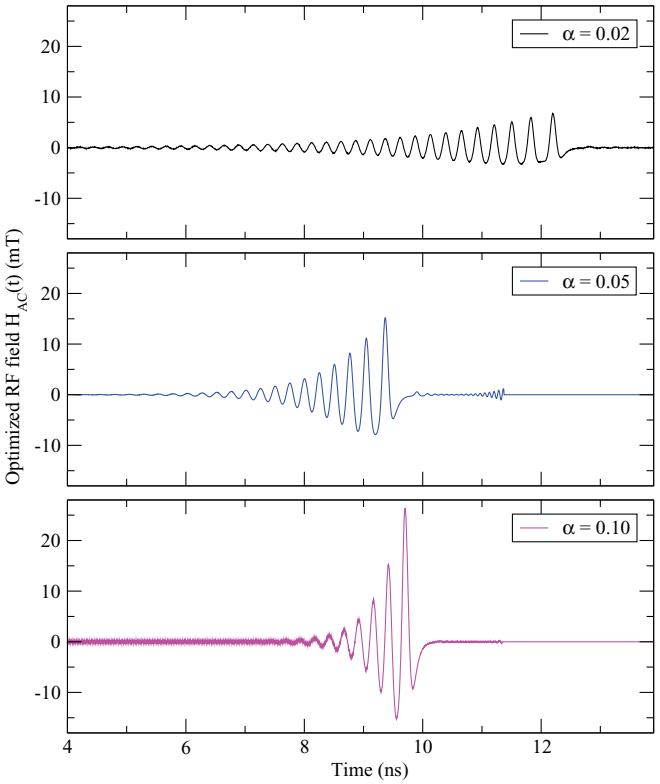

FIG. 5. (Color online) Optimized MW field obtained for different values of the damping parameter α.

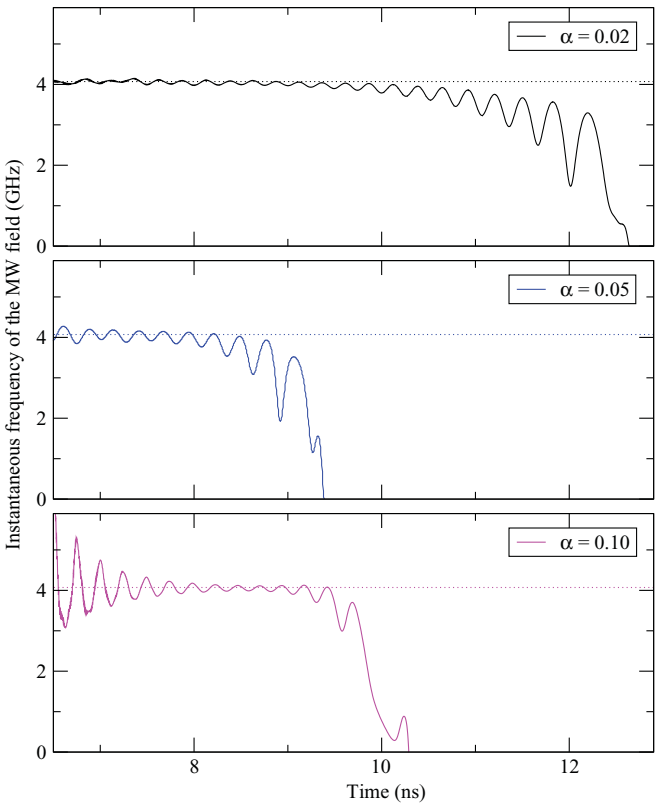

FIG. 6. (Color online) Instantaneous frequency of the MW field optimized for several values of the damping parameter α. Dotted line: FMR frequency.

This is the SW astroid. Due to the energy brought into the system by MWs, the field required for switching is smaller. This has been nicely demonstrated using the micro-SQUID technique on a 20-nm cobalt particle.[6] The most striking feature of the SW astroid obtained by these measurements is its jaggedness. In other words, the reduction of the switching field is not uniform and presents a kind of "fractal" character. The global features depend on several physical parameters, such as the MW field pulse duration, its rising time, its frequency, the dc field amplitude, and the damping parameter. In the present work, and in the particular case considered here, namely that of uniaxial anisotropy, we first wanted to check whether this reduction of the switching field is recovered by our optimal-control method. Furthermore, we address the question as to whether the SW astroid may be used as a fingerprint of a given nanocluster. More precisely, the question is whether a given SW astroid can provide us with specific information about the corresponding cluster, like its energy potential and the physical parameters such as damping.

Accordingly, we check whether a MW field $\mathbf{h}^0_{\rm ac}(t)$, which is optimized in the presence of a reference applied dc field $\mathbf{h}^0_{\rm dc}(t)$ with given direction and magnitude, for example, $h_{\rm dc} = 0.5$ and an angle of 170° with respect to the easy axis, can still induce magnetization switching in the presence of another dc field with different direction and/or magnitude. To answer this question, the MW field $\mathbf{h}^0_{\rm ac}(t)$ was used in the DLLE (7) and the calculation of the switching field was performed for several intensities and directions of the static field $\mathbf{h}$ leading to the switching curves in the presence of $\mathbf{h}^0_{\rm ac}(t)$ as shown in Fig. 7.

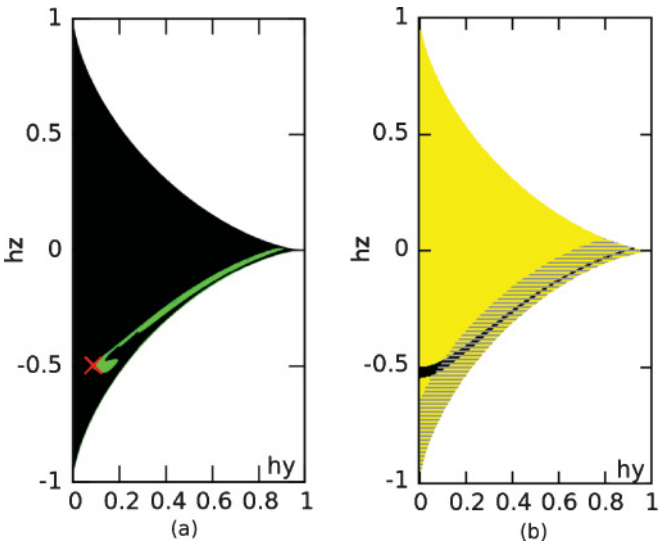

FIG. 7. (Color online) (a) Switching curve computed in the presence of the MW field $\mathbf{h}^0_{\rm ac}(t)$. The red cross indicates the amplitude and direction of the dc field for which the MW field was optimized. The area in green is where switching has been achieved, the black area is where there is no switching, and in the white area the static field is higher than the switching field (i.e., beyond the metastability region). (b) In the black area the FMR frequency is the same as for the reference dc field $\mathbf{h}^0_{\rm dc}$. In the hatched area the energy barrier between the metastable minimum and the saddle point (computed numerically) is smaller than for the reference dc field $\mathbf{h}^0_{\rm dc}$.

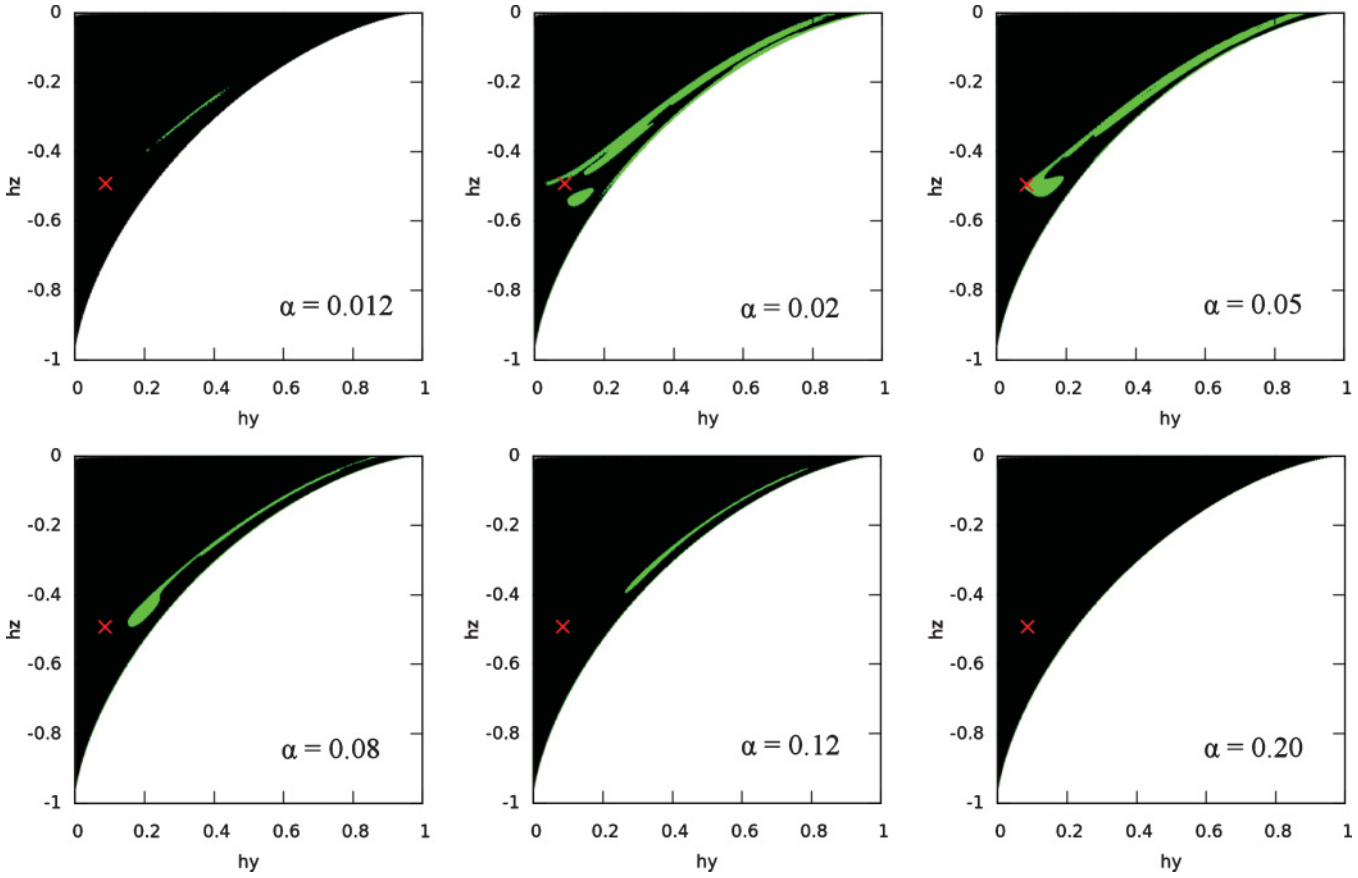

FIG. 8. (Color online) Switching curves obtained for different values of the damping parameter α with the MW field optimized for $h_{\rm dc} = 0.5$ and an angle of 170° with respect to the easy axis and $\alpha^0 = 0.05$. The color code is similar to that in Fig. 7.

As can be seen, the magnetization switching occurs only inside the golf-club-shaped green area [see Fig. 7 (left)]. In the black area, the pumping by the MW field is inefficient and switching does not occur. This curve is in agreement with the experimental data of Ref. 9.

The shape of the green pattern can be explained based on qualitative arguments about the frequency and magnitude of the MW field. As has been seen previously, in order to achieve the switching the MW field must fulfill the following conditions: (i) it must be synchronized with the proper precession frequency of the magnetization so that at short times its frequency must match the FMR frequency of the system, and (ii) the injected energy must be sufficient to overcome the energy barrier between the metastable minimum and the saddle point.

For any magnitude or direction of the field $\mathbf{h}_{\rm dc}$, both the FMR frequency and the energy barrier can be computed numerically [see Fig. 7 (right)]. In the black area the value of the FMR frequency is the same as for $\mathbf{h}^0_{\rm dc}$. In the hatched area the energy barrier is lower than for the $\mathbf{h}^0_{\rm dc}$. Outside the black zone the MW field is not synchronized with the precession frequency of the system and the switching cannot occur. Outside the hatched area the injected energy is not sufficient to overcome the energy barrier. Consequently, the switching is only achieved in the intersection between both areas. Indeed, comparing with Fig. 7 (left), this intersection matches more or less the green zone where the switching occurs.

Next, we optimize the MW field $\mathbf{h}^0_{\rm ac}(t)$ for the reference dc field $\mathbf{h}^0_{\rm dc}(t)$ with magnitude $h_{\rm dc} = 0.5$ and angle of 170° with respect to the easy axis and damping $\alpha^0 = 0.05$; then we compute the SW astroid for other values of α in the presence of the same dc and MW fields. The results are shown in Fig. 8.

We see that the shape of the switching area strongly depends on the damping parameter α. The largest green area is found for $\alpha = \alpha^0$. Then, as α increases the green area shrinks and vanishes for $\alpha > 0.12$. Indeed, for high values of α the MW field is not strong enough to compensate for the effect of damping. The same phenomenon is observed for small values of α in which case the MW field "overcompensates" for the effect of damping and thereby the energy cannot be pumped into the system in an efficient manner.

IV. CONCLUSIONS AND OUTLOOK

We have developed a general and efficient method for determining the characteristics (pulse shape, duration, intensity, and frequency) of the MW field that triggers the switching of a nanomagnet in an oblique static magnetic field. We have applied the method to the case of uniaxial anisotropy and investigated the effect of the dc field and damping on the optimized MW field. We have shown that our method does recover the switching field curves as observed on cobalt

nanoclusters. It remains though to investigate the origin of the "fractal" character observed in the measured switching curves.

We have shown that the MW field that triggers the magnetization switching, while minimizing the absorbed energy, can be efficiently calculated using the optimal control theory. According to our results, the optimal MW field is modulated both in frequency and in magnitude. The role of this MW field is to drive the magnetization toward the saddle point, then damping leads the magnetic moment to the stable equilibrium position. For the pumping to be efficient, the MW field frequency must match the proper precession frequency of the magnetization, which depends on the magnitude and the direction of the static field. Moreover, the intensity depends on the damping parameter. This result could be used to probe the damping parameter in experimental nanoparticles.

The present method is quite versatile and can be extended to other anisotropies. It could also be used to study the dynamics of nanoclusters in the many-spin approach.[19] In this case one will probably have to deal with a nonuniform MW field, especially if surface anisotropy is taken into account.[23] One may then study switching via internal spin wave excitations and the effect of the MW field on the corresponding relaxation rate.[24] Thermal effects can also be accounted for by adding a Langevin field on top of the dc and MW fields. In this case it will be interesting to investigate the interplay between the MW field and the Langevin field and to figure out when these two fields play concomitant roles.

ACKNOWLEDGMENTS

We are grateful to our collaborators E. Bonet, R. Picquerel, C. Thirion, W. Wernsdorfer (Institut Néel, Grenoble), and V. Dupuis (LPMCN, Lyon) for instructive discussion of their experiments on isolated nanoclusters. This work has been funded by the collaborative program PNANO ANR-08-P147-36 of the French Ministry.

[1] L. He *et al.*, J. Magn. Magn. Mater. **155**, 6 (1996).
[2] G. Woltersdorf and Ch. H. Back, Phys. Rev. Lett. **99**, 227207 (2007); J. Podbielski, D. Heitmann, and D. Grundler, *ibid*. **99**, 207202 (2007); Z. Wang, K. Sun, W. Tong, M. Wu, M. Liu, and N. X. Sun, Phys. Rev. B **81**, 064402 (2010).
[3] B. Meerson and L. Friedland, Phys. Rev. A **41**, 5233 (1990).
[4] W.-K. Liu, B. Wu, and J.-M. Yuan, Phys. Rev. Lett. **75**, 1292 (1995).
[5] J.-M. Yuan and W.-K. Liu, Phys. Rev. A **57**, 1992 (1998).
[6] G. Marcus, L. Friedland, and A. Zigler, Phys. Rev. A **69**, 013407 (2004); G. Marcus, A. Zigler, and L. Friedland, Europhys. Lett. **74**, 43 (2006).
[7] S. Chelkowski, A. D. Bandrauk, and P. B. Corkum, Phys. Rev. Lett. **65**, 2355 (1990).
[8] S. G. Schirmer, H. Fu, and A. I. Solomon, Phys. Rev. A **63**, 063410 (2001).
[9] C. Thirion, W. Wernsdorfer, and D. Mailly, Nature (London) **2**, 524 (2003); C. Raufast, Ph.D. thesis, Université Claude Bernard Lyon I (2007); A. Tamion, C. Raufast, E. Bonet, V. Dupuis, T. Fournier, C. Crozes, E. Bernstein, and W. Wernsdorfer, J. Magn. Magn. Mat. **322**, 1315 (2010).
[10] S. I. Denisov, T. V. Lyutyy, and P. Hänggi, Phys. Rev. Lett. **97**, 227202 (2006).
[11] G. Bertotti, I. Mayergoyz, and C. Serpico, J. Appl. Phys. **91**, 7556 (2002).
[12] Z. Z. Sun and X. R. Wang, Phys. Rev. B **74**, 132401 (2006).
[13] I. Mayergoyz, M. Dimian, G. Bertotti, and C. Serpico, J. Appl. Phys. **95**, 7004 (2004); **97**, 10A703 (2005).
[14] A. E. Bryson Jr. and Y.-C. Ho, *Applied Optimal Control: Optimization, Estimation, and Control* (Taylor and Francis, New York, 1975).
[15] A. P. Pierce, M. A. Dahleh, and H. Rabitz, Phys. Rev. A **37**, 4950 (1988).
[16] H. Jirari and W. Pötz, Phys. Rev. A **72**, 013409 (2005); **74**, 022306 (2006).
[17] M. Jamet, W. Wernsdorfer, C. Thirion, D. Mailly, V. Dupuis, P. Mélinon, and A. Pérez, Phys. Rev. Lett. **86**, 4676 (2001).
[18] L. S. Pontryagin, V. G. Boltyanskii, R. V. Gamkrelidze, and E. F. Mishchenko, *The Mathematical Theory of Optimal Processes* (Interscience, New York, 1962).
[19] H. Kachkachi and D. A. Garanin, in *Surface Effects in Magnetic Nanoparticles*, edited by D. Fiorani (Springer, Berlin, 2005), p. 75.
[20] W. H. Press, S. A. Teukolsky, W. T. Vetterling, and B. P. Flannery, *Numerical Recipes in C++: The Art of Scientific Computing* (Cambridge University Press, Cambridge, 2002).
[21] G. Girolami and D. Vakman, Meas. Sci. Technol. **13**, 909 (2002).
[22] J. C. Goswami and A. E. Hoefel, Signal Process. **84**, 1423 (2004).
[23] H. Kachkachi and M. Dimian, Phys. Rev. B **66**, 174419 (2002); D. A. Garanin and H. Kachkachi, Phys. Rev. Lett. **90**, 65504 (2003).
[24] D. A. Garanin, H. Kachkachi, and L. Reynaud, Europhys. Lett. **82**, 17007 (2008); D. A. Garanin and H. Kachkachi, Phys. Rev. B **80**, 014420 (2009).